The effect of Southern Ocean topography on the global MOC and abyssal water mass distribution

Tatsu Monkman[a] Malte F. Jansen[a]

[a] *The University of Chicago*

Corresponding author: Tatsu Monkman, tdmonkman@uchicago.edu

Early Online Release: This preliminary version has been accepted for publication in *Journal of Physical Oceanography*, may be fully cited, and has been assigned DOI 10.1175/JPO-D-23-0253.1. The final typeset copyedited article will replace the EOR at the above DOI when it is published.

ABSTRACT: We investigate the role of Southern Ocean topography and wind stress in the deep and abyssal ocean overturning and water mass composition using a suite of idealized global ocean circulation models. Specifically, we address how the presence of a meridional ridge in the vicinity of Drake Passage and the formation of an associated Southern Ocean gyre influences the water mass composition of the abyssal cell. Our experiments are carried out using a numerical representation of the global ocean circulation in an idealized two-basin geometry under varying wind-stress and Drake Passage ridge height. In the presence of a low Drake Passage ridge the overall strength of the meridional overturning circulation is primarily influenced by wind stress, with a topographically-induced weakening of the mid-depth cell and concurrent strengthening of the abyssal cell occurring only after ridge height passes 2500m. Passive tracer experiments show that a strengthening mid-depth cell leads to increased abyssal ventilation by North Atlantic water masses, as more North Atlantic Deep Water (NADW) enters the Southern Ocean and then spreads into the Indo-Pacific. We repeat our tracer experiments without restoring in the high-latitude Southern Ocean in order to identify the origin of water masses that circulate through the Southern Ocean before sinking into the abyss as Antarctic Bottom Water. Our results from these "exchange" tracer experiments show that an increasing ridge height in Drake Passage and the concurrent gyre spin-up lead to substantially decreased NADW-origin waters in the abyssal ocean, as more surface waters from north of the ACC are transferred into the Antarctic Bottom Water formation region.

Accepted for publication in *Journal of Physical Oceanography*. DOI 10.1175/JPO-D-23-0253.1.

SIGNIFICANCE STATEMENT: The objective of this study is to investigate how topographic features in the Southern Ocean can affect the overall structure of Earth's large-scale ocean circulation and the distribution of water masses in the abyssal ocean. We focus on the Southern Ocean because the region is of central importance to both exchange between the Atlantic and Indo-Pacific ocean basins and for CO2 and heat uptake into the abyssal ocean. Our results indicate that Southern Ocean topography plays a major role in the overall circulation by a) controlling the direct transfer of abyssal waters from the Atlantic to the Indo-Pacific via its influence on the Atlantic meridional overturning circulation, and b) controlling the coupling between the abyssal ocean and surface waters north of the Antarctic Circumpolar Current via the Southern Ocean gyre.

1. Introduction

The meridional overturning circulation (MOC) is a large-scale ocean circulation pattern driven by winds, buoyancy gradients, and vertical mixing that transports heat and tracers polewards and facilitates heat and carbon transport into the deep and abyssal ocean (Toggweiler et al. 2006; Anderson et al. 2009; Ito et al. 2010). Within the MOC, the Southern Ocean plays a central role by facilitating the return of dense Atlantic and Indo-Pacific waters to the ocean surface via wind-driven upwelling along the length of the Antarctic Circumpolar Current (ACC). The Southern Ocean circulation governs the exchange of water masses between the Atlantic and Indo-Pacific ocean basins (Talley 2013; Jones and Cessi 2016; Thompson et al. 2016; Ferrari et al. 2017) and has particular importance in setting the strength of the adiabatic circulation of the mid-depth cell (Toggweiler and Samuels 1995a; Vallis 2000; Wolfe and Cessi 2011), which in turn plays a critical role in oceanic heat transport and the broader climate (Srokosz et al. 2012). However, despite the Southern Ocean's importance to Earth's climate, our theoretical understanding of the structure of its circulation remains largely limited to zonally-integrated theory. For example, the relationship between submarine topography in the Southern Ocean and localized deep water upwelling has only recently been characterized in GCMs (Tamsitt et al. 2017; Youngs and Flierl 2023) and the role of Southern Ocean topography in the global MOC has only relatively recently become a focus of theoretical research (Nadeau and Ferrari 2015; Kong and Jansen 2021; Youngs and Flierl 2023). Here, we build upon these recent advancements and investigate the relationship between zonal

Accepted for publication in *Journal of Physical Oceanography*. DOI 10.1175/JPO-D-23-0253.1.

topographic asymmetries in the Southern Ocean and the water mass composition of the abyssal ocean from an idealized perspective.

In the zonally integrated picture of the two-cell MOC, zonal wind-stress forcing along the length of the Southern Ocean channel drives an equator-ward transport of surface waters that is balanced by deep water upwelling along tilted isopycnals in the Southern Ocean (Toggweiler and Samuels 1995a; Wolfe and Cessi 2011; Nikurashin and Vallis 2012). This wind-driven transport is partially compensated by baroclinic eddies, which act to flatten the isopycnals and transport upwelled deep waters poleward (Marshall and Radko 2003). The residual circulation that results from these two processes governs the pathway of tracers as they upwell adiabatically along isopycnals to the surface of the Southern Ocean (Walin 1982; Gnanadesikan 1999; Nikurashin and Vallis 2012; Marshall and Speer 2012). The upwelling deep water, commonly referred to as Circumpolar Deep Water (CDW), consists of both former North Atlantic Deep Water (NADW) that forms due to buoyancy loss in the North Atlantic as well deep waters from the Indo-Pacific return branch of the abyssal cell (Lumpkin and Speer 2007; Marshall and Speer 2012).

Once upwelled CDW reaches the surface of the Southern Ocean it travels either southward towards the bottom water formation regions off the coast of Antarctica, entering the abyssal cell, or northwards to close the upper branch of the mid-depth cell (Talley 2013). Ferrari et al. (2014) suggests that the sign of the yearly-averaged buoyancy flux over the deep water upwelling regions determines the direction of this surface flow, with surface flow directed poleward in regions of net negative surface buoyancy flux and equatorward in regions of net positive buoyancy flux, with the horizontal extent of the two regions largely determined by the quasi-permenant (summer) sea ice extent around Antarctica. In the current climate, a large proportion of mid-depth NADW is thus thought to upwell to the south of the positive-negative buoyancy flux transition and flow into the abyssal cell, leading to a configuration referred to as the "figure eight" circulation by Talley (2013) and Ferrari et al. (2014) whereby the mid-depth cell exchanges its densest water masses with the lightest water masses of the abyssal cell in the Southern Ocean (Lumpkin and Speer 2007; Talley 2013). CDW sourced from the Indo-Pacific abyssal circulation is thought to upwell in regions of both positive and negative buoyancy restoring and is thus split between the bottom water formation regions in the South and the surface and intermediate waters to the north of the ACC (Talley 2013; Cessi 2019).

Accepted for publication in *Journal of Physical Oceanography*. DOI 10.1175/JPO-D-23-0253.1.

Recent studies point towards the importance of topographic zonal asymmetries for water mass pathways in the Southern Ocean, although it remains unclear how these zonal asymmetries affect our theoretical picture of the global MOC. Both outcropping and submarine topographic features are present in the Southern Ocean, which are associated with large-scale standing meanders in the ACC (Thompson and Garabato 2014), gyres (Nadeau and Ferrari 2015; Patmore et al. 2019), and AABW export (Stewart and Hogg 2017; Schmidgall et al. 2023). Topographically-induced standing meanders and gyres are thought to carry a significant amount of surface water towards bottom water formation regions (Schröder and Fahrbach 1999; Reeve et al. 2019) and have been shown to facilitate a large portion of southward oceanic heat transport in idealized, eddy-resolving models (Wilson et al. 2022; Xing et al. 2023). Studies such as Tamsitt et al. (2017) and Youngs and Flierl (2023) further suggest that deep water upwelling in the Southern Ocean is highly localized near submarine topography, a fact that is obscured in the zonally integrated view and largely ignored in zonally symmetric theory. How these zonal topographic asymmetries affect our idealized theoretical view of the global overturning circulation and water mass properties remains unclear.

A deeper understanding of the role of zonal topographic asymmetries in the Southern Ocean's circulation has implications for our understanding of past climates. The tectonic opening of the Tasmanian Gateway and Drake Passage and the concurrent formation of the ACC are thought to have played a key role in the dramatic global cooling experienced during the early Cenozoic and the glaciation of Antarctica (Kennett 1977; Zachos et al. 2001), although the role of these topographic changes relative to atmospheric CO_2 drawdown during the Eocene-Oligocene transition is uncertain (Goldner et al. 2014; Anagnostou et al. 2016; Toumoulin et al. 2020). The unblocking of the Southern Ocean and rise of the ACC have also more directly been linked to the formation and strengthening of the mid depth cell in the Atlantic (Toggweiler and Bjornsson 2000; Sijp and England 2004), reduced southward heat transport by subpolar gyres and subsequent Southern Ocean cooling (Sauermilch et al. 2021), and to Antarctic Bottom Water formation (Kennedy et al. 2015), although the exact mechanisms at play can be difficult to extract from complex coupled climate models. Thus in this study we attempt to isolate the effect of changing Southern Ocean topography on the global ocean circulation by considering the effect of changing Drake Passage ridge heights in a highly simplified setting.

Accepted for publication in *Journal of Physical Oceanography*. DOI 10.1175/JPO-D-23-0253.1.

Here we investigate the influence of Southern Ocean topography on the global ocean circulation in an idealized two-basin ocean model, paying particular attention to the effect of Southern Ocean topography on the strengths of the overturning cells and on the water mass composition of the abyssal ocean. For simplicity we limit our study to modifying the height of a meridional ridge in the vicinity of Drake Passage and measuring its effects on the large-scale circulation under various wind stress forcings. We employ passive tracers in a setup similar to that of Jones and Abernathey (2019) (see also Haine and Hall 2002; Primeau 2005) to characterize the response of the deep ocean water mass composition to changes in topography and wind stress. Finally, we introduce "exchange" tracers which are not subject to restoring at the surface of the Southern Ocean, allowing us to identify the origin of the upwelled deep waters and surface waters that supply bottom water formation at the surface south of the ACC.

Our results indicate that the addition of a meridional ridge in Drake Passage can significantly alter the structure of the large-scale ocean circulation by weakening the mid-depth cell and by spinning up a Southern Ocean gyre. Furthermore, our tracer experiments indicate that such circulation shifts can have a large impact on the water mass composition of the abyssal ocean, leading to decreased direct transfer of NADW between the Atlantic and Indo-Pacific and increased entrainment of surface tracers southwards across the ACC into the AABW formation sites.

2. Methods

a. Model setup and experiments

We employ an idealized, ocean-only GCM to simulate the response of an Earth-like MOC to changes in Southern Ocean topography and wind stress forcing. We use the Massachusetts Institute of Technology General Circulation Model (MITgcm) (Marshall et al. 1997) with a horizontal domain that consists of a spherical sector extending from $70^o S$ to $70^o N$ in the meridional and 210^o in the zonal directions, with a horizontal resolution of $2^o x 2^o$ (equivalent to a meridional grid spacing of $\sim$ 200km and a zonal grid spacing that ranges from $\sim$ 80km at the northern and southern ends of the domain to $\sim$ 220km at the equator). Our models are thus not eddy resolving and rely on parameterizations to capture the effects of mesoscale eddies, a tradeoff that is discussed further in the limitations section. The vertical domain is 4000 m deep and consists of 40 vertical levels of varying thickness, from 37 meters at the surface to 159 meters at the bottom.

Accepted for publication in *Journal of Physical Oceanography*. DOI 10.1175/JPO-D-23-0253.1.

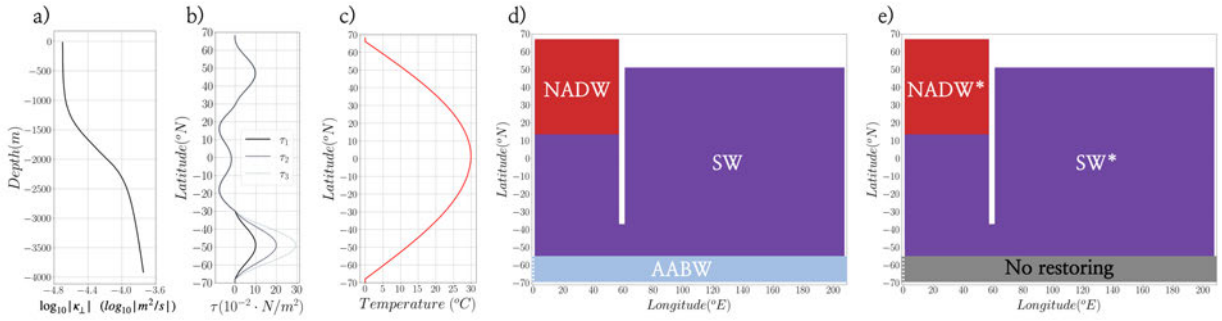

FIG. 1. Simulation setup. a) Vertical diffusivity profile used for tracer and buoyancy diffusion. b) Meridional, zonally symmetric zonal wind stress profile, including modified wind stress forcings over the Southern Ocean. c) Meridional, zonally symmetric surface temperature restoring profile in ^oC. d) Surface regions corresponding to surface restoring fields for ventilation tracers "NADW", "AABW", and "SW" (reflecting "North Atlantic Deep Water," "Antarctic Bottom Water," and "Surface Water" ventilation tracers, see methods). Ventilation tracers are restored to 1 at the surface in regions labeled here and zero elsewhere. e) Surface regions corresponding to surface restoring fields for exchange tracers "NADW*" and "SW*" (reflecting "North Atlantic Deep Water"and "Surface Water" exchange tracers, see methods). Exchange tracers are restored to 1 over the labeled regions shown, are not restored over the grey-shaded area in the Southern Ocean, and are restored to zero elsewhere. Dashed white lines near the southern end of the domain show the location of the Southern Ocean ridge.

We apply a simplified, Earth-like topography consisting of a reentrant channel along the southern end of the domain extending from 68^oS to 56^oS, and two ocean basins to the north: a narrow ocean basin extending to 68^oN, and a wide basin to 50^oN (for brevity we refer to these basins as the "Southern," "Atlantic," and "Indo-Pacific" Oceans, respectively). The basins are separated by a long continent of 4^o zonal width centered at 0^oE extending from 56^oS to 68^oN representing the Americas and a short continent of 4^o zonal width centered at 60^oE extending from 36^oS to 68^oN representing Africa / Eurasia. This topographic setup is based on studies such as Jones and Abernathey (2019), Baker et al. (2020), and Nadeau and Jansen (2020), all of which successfully recreate an Earth-like two-cell MOC. For simplicity, we limit additional Southern Ocean topography to a meridional ridge of 4^o zonal width of varying heights centered at 0^oE and spanning across Drake Passage.

We use a linear, temperature-only equation of state such that buoyancy is given by $b = g\alpha\theta$, where $g = 9.81m/s^2$ is gravitational acceleration, $\alpha = 2 \cdot 10^{-4}K^{-1}$ is the thermal expansion coefficient and θ is potential temperature. Temperature and passive tracers are advected using the Prather

Accepted for publication in *Journal of Physical Oceanography*. DOI 10.1175/JPO-D-23-0253.1.

(1986) second-order moments advection scheme. The unresolved eddy-induced advection is parameterized via the Gent and Mcwilliams (1990) (GM) scheme and isopycnal and diapycnal mixing is parameterized via a rotated diffusivity tensor, following Redi (1982). The along-isopycnal diffusivity and GM coefficient are spatially constant $1000 m^2/s$, while the vertical diffusivity increases with depth to simulate enhanced deep and abyssal ocean mixing due to turbulent wave breaking (Figure 1a). We force the model with zonally uniform wind stress and temperature restoring fields, both broadly based on observations (Figure 1bc) and similar to the temperature and wind-stress forcing fields used in Jones and Cessi (2016) and Nadeau and Jansen (2020). The surface temperature restoring time is 30 days across all models.

We configure all models using the setup described above but with varying wind stress maximums over the Southern Ocean (Figure 1b) and ridge heights in Drake Passage (Figure 1de). We test three different wind stress cases: a low wind case with Southern Ocean wind stress maximum of $\tau_1 = 0.1 N/m^2$, a medium wind stress maximum of $\tau_2 = 0.2 N/m^2$, and a high wind stress maximum of $\tau_3 = 0.3 N/m^2$. We test our model's response to each of these wind stress cases under 6 different Drake Passage ridge heights (0m, 1000m, 2000m, 2500m, 3000m, 3500m), for a total of 18 model setups. All models are spun up from rest for at least 12,000 years until equilibrium (when temporal variations in both tracer and temperature fields are negligible) has been reached. All simulations have deep/bottom water formation (defined as deep convection reaching depths $> 1 km$) in two regions: the North Atlantic north of 64°N and the Southern Ocean south of $66° S$ between $0° E$ and $10° E$.

b. Passive tracers

In addition to temperature, we employ five passive tracers to track the pathways of water masses through the global circulation. We apply three "ventilation" tracers that track the pathways of water that originates at the surface of the North Atlantic (which broadly captures the production of North Atlantic Deep Water, and is hereafter referred to as "NADW"), in the Southern Ocean in the latitude range of Drake Passage (which broadly captures the production of Antarctic Bottom Water, and is hereafter referred to as "AABW")[1], and over the remainder of the global ocean,

[1] Note that the restoring fields for "NADW" and "AABW" presented here encompass much larger horizontal domains than the actual deep water formation sites occupy in our models. Despite this, we have found that the abyssal Indo-Pacific ventilation tracer concentrations for AABW and NADW are generally unchanged if the restoring is applied over more restrictive areas, and choose the above restoring fields for easy comparison with the "exchange" tracers.

Accepted for publication in *Journal of Physical Oceanography*. DOI 10.1175/JPO-D-23-0253.1.

including the entire Indo-Pacific and the northern Southern Ocean (for simplicity we refer to this water mass as "surface water," or "SW"). Each ventilation tracer is restored to 1 over different regions of the ocean surface and zero everywhere else (Figure 1d). Similar to the setup used in Jones and Abernathey (2019) the restoring fields for NADW, SW, and AABW are non-overlapping and together cover the entire ocean surface. The restoring time for passive tracers at the surface is 5.8 days.

We introduce additional "exchange" tracers (hereafter referred to as NADW* and SW*) which allow us to separate AABW into contributions from former NADW versus other lower latitude sources. The restoring fields of NADW* and SW* mirror those of the ventilation NADW and SW tracers but with no restoring applied in the latitudes of Drake Passage (Figure 1e). Removing the surface restoring condition in the Southern Ocean allows NADW* and SW* tracers to surface along the upwelling branch of the Southern Ocean MOC and reenter the abyssal ocean via the abyssal water formation regions off the coast of Antarctica. The concentration of NADW* in the abyssal ocean therefore describes both NADW that reaches the abyssal ocean via internal pathways and any NADW that upwells in the Southern Ocean and renters the abyssal ocean via deep water formation regions.

The exchange tracer concentration in the abyssal Indo-Pacific measures the relative importance of the advective pathway of former NADW into the abyssal cell versus diffusive ventilation in the Indo-Pacific. In the perfect "figure 8" limit (Ferrari et al. 2017; Nadeau and Jansen 2020), where NADW is entirely transformed into AABW around Antarctica (where NADW* is not restored in our models) we would expect the abyssal Indo-Pacific to be mostly NADW* with any abyssal SW* concentration the result of downwards diffusion in the Indo-Pacific, a process that is expected to be less efficient than the advective pathway. If, by contrast, all NADW that enters the Southern Ocean returns northward in the Atlantic, thereby creating two separate overturning cells, the exchange tracer in the abyssal Indo-Pacific would only be ventilated by diffusion and thus be dominated by SW*.

We note that both the ventilation and exchange tracer concentrations should each sum up to 1 in each grid cell. However in practice we find that ventilation tracers experience some degree of loss such that their sum is slightly less than 1 within the abyssal ocean (See Figure 5 in Section

Accepted for publication in *Journal of Physical Oceanography*. DOI 10.1175/JPO-D-23-0253.1.

4). The exact source of this discrepancy is difficult to verify, and may be the result of incomplete equilibration, surface restoring, and/or numerical inaccuracies.

c. Circulation response to wind stress and topographic forcing

We characterize the strength of the ACC using the barotropic streamfunction given by:

$$\psi_{bt}(x,y) = \int_{y=y}^{y=68^oN} \int_{-H}^{0} \overline{u}(x,y,z)dzdy, \tag{1}$$

where H is the ocean depth, $\overline{u}(x,y,z)$ is the time averaged local eulerian velocity in the zonal direction taken over the last 50 years of our simulations (although we note that due to the non-eddy resolving resolution and time-constant boundary conditions there is no significant temporal variability in our simulations once equilibrated). The addition of a meridional ridge in the vicinity of Drake Passage forces a subpolar gyre south of the ACC and to the east of Drake Passage in a geographically similar location to the Weddell Gyre[2]. As in Patmore et al. (2019) we define the strength of the ACC as the net barotropic transport across Drake Passage:

$$\psi_{acc} = \psi_{bt}(0^oE, 68^oS), \tag{2}$$

and define the strength of the subpolar Southern Ocean gyre as the difference between the maximum barotropic stream function in the latitude band of Drake Passage, $\max\left|\psi_{bt}(x,y)\right|_{y=68^oS}^{y=54^oS}$, and the ACC transport:

$$\psi_{gyre} = \max\left|\psi_{bt}(x,y)\right|_{y=68^oS}^{y=54^oS} - \psi_{acc}. \tag{3}$$

Note that here and throughout our study we focus on the effects of the subpolar gyre that forms to the south of the ACC. Gyre circulations to the north of the ACC, such as the Southern Ocean "supergyre" (Ridgway and Dunn 2007; Speich et al. 2007), may also affect the inter-basin exchange but are not explored here.

[2]We note that while the subpolar gyre generated in our simulations shares features with the real Weddell and Ross Gyres, it represents a significant simplification of the gyre dynamics in the real southern Ocean. In particular, the Weddell gyre is associated with an outcropping ridge to the east and both the Weddell and Ross gyres are associated with a submarine zonal barrier to the north. Furthermore, the specifics of the ocean circulation simulated in the vicinity of Southern Ocean topography may depend on the model setup, with some idealized models producing a pair of counter-rotating gyres on either side of the westerly circumpolar jet (Wilson et al. 2022). Exploring the effects of additional topographic features and different model configurations on the circulation is left for future study.

Accepted for publication in *Journal of Physical Oceanography*. DOI 10.1175/JPO-D-23-0253.1.

We quantify the response of the global overturning circulation to changes in Southern Ocean topography and wind forcing using the isopycnal MOC, $\psi(y,b)$, which gives a useful representation of the material transport pathways of the deep and abyssal ocean (Nurser and Lee 2004; Ferrari and Ferreira 2011):

$$\psi(y,b') = \int_{x_0}^{x_1} \int_{-H}^{0} (\overline{v}(x,y,z) + \overline{v}^*(x,y,z)) \mathcal{H}(b' - \overline{b}(x,y,z,t)) dx dz, \tag{4}$$

where y denotes latitude, x_0 and x_1 give the zonal extent of the ocean basin, H is the ocean depth, $\overline{v}(x,y,z,t)$ and $\overline{v}^*(x,y,z)$ are the time averaged local meridional velocity and eddy transport velocity due to the GM scheme, respectively, $\mathcal{H}$ is the heavyside step function, b' is any given buoyancy level, and $\overline{b}(x,y,z)$ is the time averaged local buoyancy. We define the strength of the mid depth cell as the the maximum strength of $\psi(y,b')$ between $b = 0.002 m/s^2$ and $b = 0.019 m/s^2$ integrated over the southern end of the Atlantic basin ($36^o S$):

$$\psi_{atl} = \max \left| \int_{2^o E}^{58^o E} \int_{-H}^{0} (\overline{v}(x,36^o S,z) + \overline{v}^*(x,36^o S,z)) \mathcal{H}(b' - \overline{b}(x,36^o S,z)) dx dz \right|_{b'=0.002 m/s^2}^{b'=0.019 m/s^2}. \tag{5}$$

Note that we choose this definition rather than using the maximum mid-depth cell strength in the North Atlantic because it is most relevant to the transport of NADW into the abyssal Indo-Pacific, discussed in Section 4. Either metric can be used to characterize the magnitude of the mid-depth cell strength and we note that the two metrics are highly correlated ($R^2 = 0.99$). We define the strength of the abyssal cell, ψ_{ip}, using the minimum value of the streamfunction in the Indo-Pacific (north of $36^o S$) between the buoyancy levels of $b = 0.0004 m/s^2$ and $b = 0.005 m/s^2$:

$$\psi_{ip} = \min \left| \min \left| \int_{62^o E}^{208^o E} \int_{-H}^{0} (\overline{v}(x,y,z) + \overline{v}^*(x,y,z)) \mathcal{H}(b' - \overline{b}(x,y,z)) dx dz \right|_{y=36^o S}^{y=50^o N} \right|_{b'=0.0004 m/s^2}^{b'=0.005 m/s^2}. \tag{6}$$

Accepted for publication in *Journal of Physical Oceanography*. DOI 10.1175/JPO-D-23-0253.1.

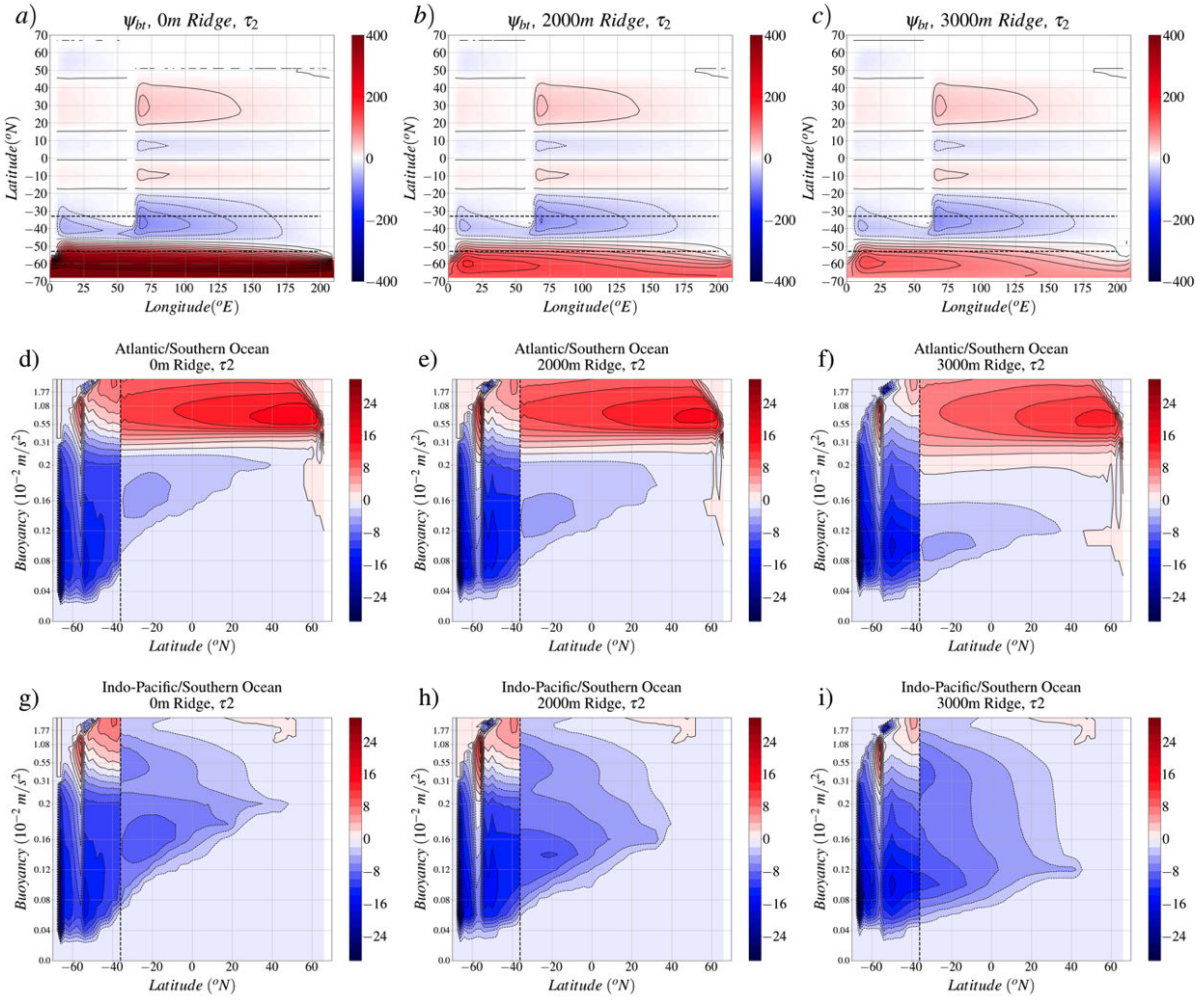

FIG. 2. Ocean circulation states for various topographic configurations in our models for (from left to right) the no ridge case, 2000 meter ridge case, and 3000 meter ridge cases, under $0.2N/m^2$ Southern Ocean maximum wind stress. a-c) barotropic stream functions. d-f) isopycnal overturning stream functions for the Atlantic (north of 36^oS) and Southern Ocean (south of 36^oS). Here the y-axis is stretched to the average z-space height of the corresponding isotherms in the Atlantic Ocean. g-j) as in d-f) but showing the Indo-Pacific overturning streamfunction north of 36^oS. Contour intervals are 10Sv for the barotropic stream functions (a-c) and 2Sv for the isopycnal meridional stream functions (d-j).

3. Results: ocean circulation

a. Barotropic circulation

The Southern Ocean's barotropic circulation is highly sensitive to both wind stress and ridge height (Figure 2a-c, Figure 3ab). The flat bottom cases exhibit a strong ACC, ranging from 228Sv

Accepted for publication in *Journal of Physical Oceanography*. DOI 10.1175/JPO-D-23-0253.1.

for $0.1N/m^2$ wind stress to 665Sv for 0.3 N/m^2 wind stress. As found in previous work (e.g. Nadeau and Ferrari 2015), the strength of the ACC shows a rapid weakening once even a modest (1000m) ridge is introduced, dropping to 93Sv for $0.1N/m^2$ wind stress and 193Sv for $0.3N/m^2$ wind stress. ACC strength falls off further as ridge height increases beyond 1000m, reaching as little as 31Sv for the 3500m ridge case (Figure 3a). Although ACC strength generally increases under larger wind stresses, this relationship weakens as ridge height increases and becomes mostly flat for the 3500m ridge height case (c.f. Kong and Jansen 2021; Shakespeare and Hogg 2012). Here it is worth noting that our model's coarse resolution does not explicitly resolve transient eddies and necessitates the use of a constant background GM diffusivity, which has been shown previously to lead to an overrepresentation of ACC sensitivity to wind stress (Mak et al. 2018; Kong and Jansen 2021), although the presence of topography has been found to significantly reduce the sensitivity of the ACC transport to mesoscale eddy representation (and hence resolution) as standing meanders modulate the effective eddy diffusivity (Kong and Jansen 2021; Stewart et al. 2023). The results of Kong and Jansen (2021) suggest that the response of the ACC transport to wind stress changes may be overestimated by almost an order of magnitude compared to eddy resolving simulations in the limit of a flat bottom. In the presence of significant topography the difference between eddy resolving and coarse resolution simulations was found to be substantially reduced (but still present), with the sensitivity to wind stress changes enhanced by up to a factor of two in coarse resolution simulations.

A Southern Ocean ridge is required for Southern Ocean gyre formation in our models. No subpolar gyre forms in the flat bottom Southern Ocean cases, while a subpolar gyre extending from the coast of Antarctica to the southern edge of the ACC forms in the lee of Drake Passage following the introduction of a 1000m ridge (Figure 2a-c). Consistent with results from previous studies (Nadeau and Ferrari 2015; Patmore et al. 2019), the Southern Ocean gyre strengthens in response to both increasing ridge height and wind stress (Figure 3b). The Southern Ocean gyre shows a strong dependance on both wind stress and ridge height, ranging in strength from 12Sv in the 1000m, $0.1N/m^2$ case to 119Sv in the 3500m, $0.3N/m^2$ case, a range that encompasses values similar to observational (Dotto et al. 2018; Reeve et al. 2019) and model-derived (Mazloff et al. 2010; Wang 2013) estimates of the strengths of the Ross and Weddell subpolar gyres.

Accepted for publication in *Journal of Physical Oceanography*. DOI 10.1175/JPO-D-23-0253.1.

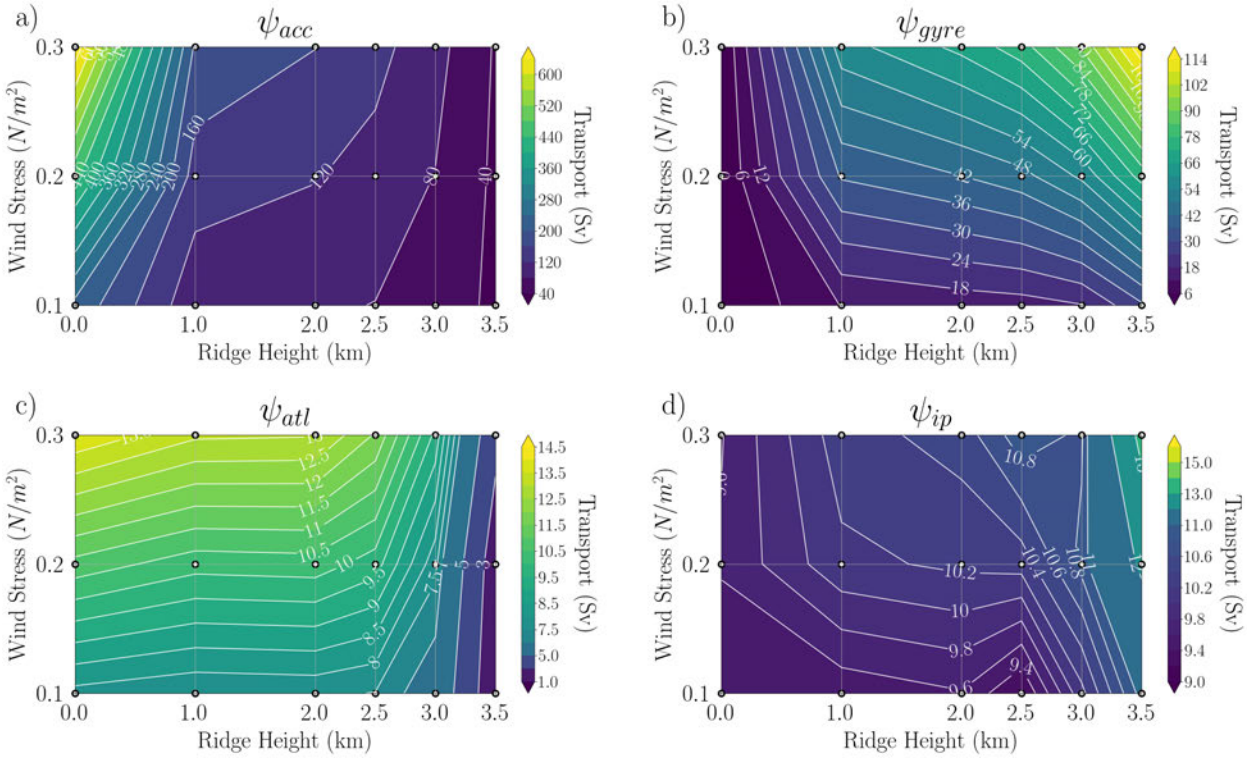

FIG. 3. Bivariate plots of MOC response to various wind-stress and ridge height configurations as functions of ridge height (in x) and wind stress (in y). a) Maximum barotropic ACC transport at Drake Passage. b) Southern Ocean gyre transport. c) Maximum mid-depth cell strength at $36^o S$. d) Maximum abyssal cell strength north of $36^o S$. Circular markers denote the wind stress / ridge height combinations used in this study.

The close relationship between the strength of the ACC / the Southern Ocean gyre and Southern Ocean submarine topography is well documented in the literature and is a consequence of the topographic form stress (Munk and Palmén 1951; Olbers 1998; Nadeau and Ferrari 2015; Patmore et al. 2019). As ridge height increases, the ACC slows and a Southern Ocean gyre forms in the lee of the meridional ridge (Abernathey and Cessi 2014), as topographic-form drag replaces bottom friction as the momentum sink balancing surface wind stress (Thompson and Garabato 2014; Patmore et al. 2019).

b. MOC

Our simulations successfully recreate the two-cell MOC structure observed in the real ocean (e.g. Lumpkin and Speer 2007; Cessi 2019), with a mid-depth cell largely confined to the narrow, active

Accepted for publication in *Journal of Physical Oceanography*. DOI 10.1175/JPO-D-23-0253.1.

basin (c.f. Jones and Cessi 2016) and an AABW-fed abyssal cell that dominates the Indo-Pacific sector. The isopycnal MOC under medium wind forcing ($\tau_2 = 0.2N/m^2$) for the 0m, 2000m, and 3000m ridge cases is shown in Figure 2d-i. Overall, the response of the overturning circulation to changes in topography and wind-stress is similar to that found by previous targeted studies of the overturning in the Southern Ocean (Toggweiler and Samuels 1995b; Abernathey et al. 2011; Kong and Jansen 2021; de Boer et al. 2022), and in single-basin models such as Chang and Jansen (2021).

The strength of the mid-depth cell at the northern end of the Southern Ocean, ψ_{atl}, is largely insensitive to ridge heights between 0m to 2000m (Figure 3c) and is instead primarily a function of the maximum wind stress over the Southern Ocean, ranging from 7.7Sv in the 2000m ridge case under low wind stress to around 13.8Sv for high wind stress in the flat-bottom case. Mid-depth cell strength falls off as ridge heights pass 2500m, reaching a minimum of 1.6Sv for the 3500m ridge case under low wind stress. An eventual fall off of the mid-depth cell strength may be expected as the topography approaches the limit of a closed Drake Passage where no or only a substantially weakened cross-equatorial mid-depth cell is expected (Bryan 1986; Toggweiler and Samuels 1995a). In our models, the onset of a substantial decline at a ridge height of 2500m is associated with the intrusion of the ridge into the depth range of the mid-depth cell in the Southern Ocean, when mid depth cell isopycnals begin to intersect with the ridge at the northern end of Drake Passage (not shown).

The strength of the abyssal cell, ψ_{ip}, varies between about 9.4 and 10.9Sv across our simulations with ridge heights $\leq 3000m$, increasing only weakly with increasing topographic height and wind stress (Figure 3d). The abyssal cell increases to 13.3Sv for the 3500m ridge case under high wind stress (c.f. Xing et al. 2023). The muted abyssal cell response over medium and low ridge heights is consistent with similar studies such as Bishop et al. (2016) and Chang and Jansen (2021), who find that the abyssal cell in the northern basins is largely dependent on the buoyancy boundary conditions over the Southern Ocean and the vertical diapycnal diffusivity in the abyss, both of which are held constant in our study. Here we note that our metric for abyssal cell strength does not capture the response of the Southern Ocean channel's maximum abyssal circulation or the net northward AABW export, both of which have been shown to be more sensitive to Southern Ocean topography (Chang and Jansen 2021; Schmidgall et al. 2023).

Accepted for publication in *Journal of Physical Oceanography*. DOI 10.1175/JPO-D-23-0253.1.

4. Results: water mass tracers

a. Tracer concentrations

Zonally-averaged time-mean tracer concentration fields in the Indo-Pacific and Southern Ocean for the middle (τ_2) wind stress case and for three different ridge heights ($0m, 2000m, 3000m$) are shown in Figure 4. NADW tracer enters the Southern Ocean at depth, visible here as the maximum in NADW concentration between 1000m-1500m in the northern Southern Ocean (Figure 4a-c), and either travels into the mid-depth Indo-Pacific via zonal exchange (Nadeau and Jansen 2020) or upwells directly to the surface of the Southern Ocean, with isopycnal mixing likely contributing to a decline in NADW concentration as it approaches the Southern Ocean surface (Jones and Abernathey 2019). The concentration of NADW ventilation tracer that reaches the abyssal Indo-Pacific (below 2000m) ranges from 4-17% (Figure 5), indicating that relatively little NADW is able to enter the Indo-Pacific directly at depth. The concentration of NADW ventilation tracer in the abyssal Indo-Pacific generally trends downwards with decreasing wind stress and higher bottom topography (Figure 5).

AABW makes up the primary component of the abyssal Indo-Pacific in all cases, with average abyssal concentrations ranging from 68% (in the 0m ridge, τ_3 wind-stress forcing case) to 93% (in the 3500m ridge, τ_1 wind-stress forcing case). AABW concentrations in the abyssal Indo-Pacific are fairly uniform (Figure 4g-i), and generally increase with ridge height and decrease with wind stress (Figure 5). Finally, SW tracer is generally limited primarily to the thermocline of the Indo-Pacific and northern Southern Ocean and falls off quickly with depth (Figure 4d-f), with mean abyssal SW concentrations in the abyssal Indo-Pacific ranging from 10% for the 0m ridge, high wind stress case, to $< 1\%$ for the 3500m ridge, low wind stress case.

NADW ventilation of the abyssal Indo-Pacific is highly correlated with the strength of the mid-depth cell at the southern end of the Atlantic (Figure 6a), which measures the volume of NADW that makes it into the Southern Ocean. SW concentration in the abyssal Indo-Pacific falls off with increasing ridge height and decreasing wind stress and is highly correlated with ψ_{surf} (Figure 6b), the net rate of subduction by the upper branch of the mid-depth cell in the Southern Ocean. We diagnose ψ_{surf} as the maximum stream function at the bottom of the surface layer in the Southern

Accepted for publication in *Journal of Physical Oceanography*. DOI 10.1175/JPO-D-23-0253.1.

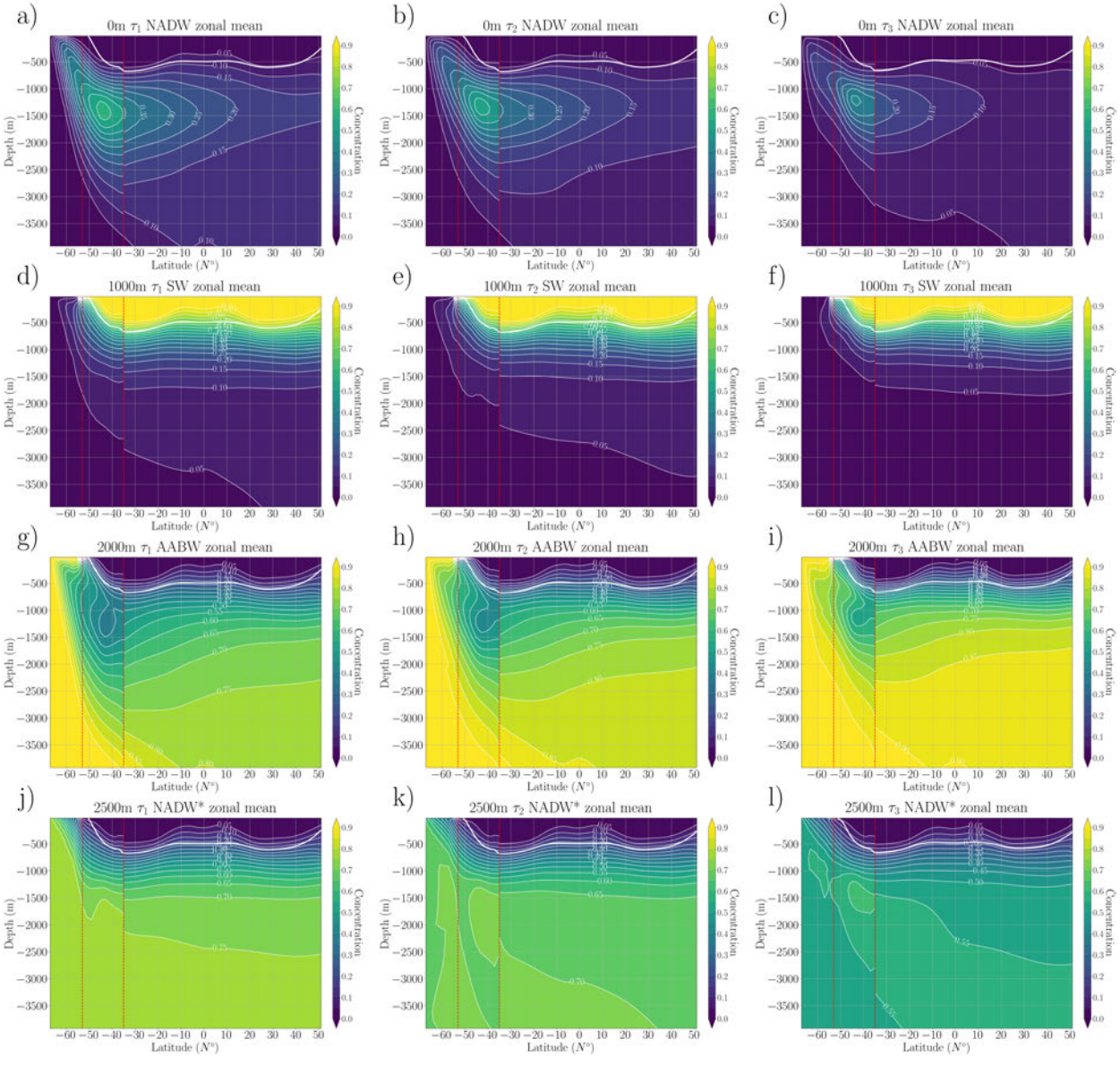

FIG. 4. Zonally averaged tracer concentrations over the Southern Ocean (south of 36^oS) and Indo-Pacific (north of 36^oS) for NADW (a-c), SW (d-f), AABW (g-i), and NADW* (j-l) for 0m, (left), 2000m (center) and 3000m (right) topograpgy and with $\tau = 0.2N/m^2$ wind stress. Vertical dashed lines at 54^oS and 35^oS give the northern latitudinal extent of "Drake Passage" (i.e., the southern tip of the long continent) and the latitude of "Cape Horn" (i.e., the southern tip of the short continent), respectively. The solid white line indicates the isopycnal corresponding to the minimum buoyancy outcrop in the Southern Ocean, $b_{SO_{min}}$.

Ocean north of Drake Passage:

$$\psi_{surf} = \max |\psi(y, b_{s_{min}})|_{y=54^oS}^{y=32^oS}, \tag{7}$$

Accepted for publication in *Journal of Physical Oceanography*. DOI 10.1175/JPO-D-23-0253.1.

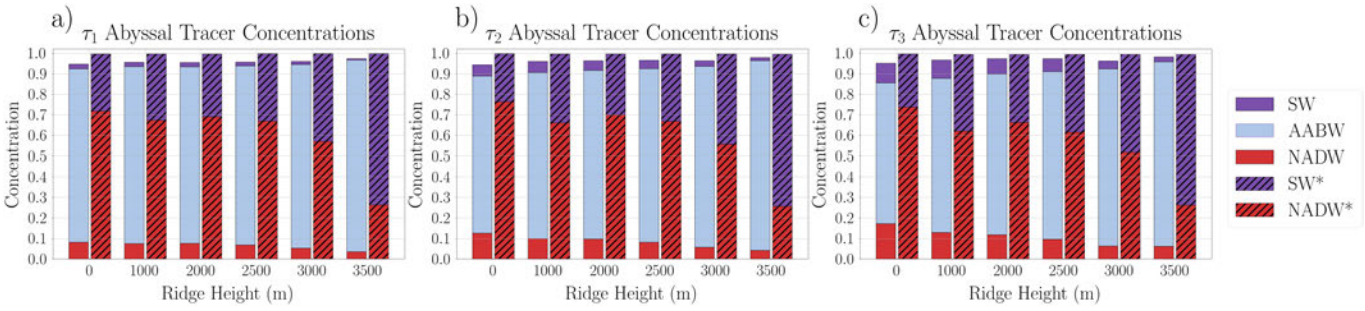

FIG. 5. Horizontally-averaged time-mean ventilation and exchange tracer concentrations in the abyssal Indo-Pacific below 2000m. Ventilation tracer concentrations are given by SW (Surface Water, solid purple), AABW (Antarctic Bottom Water, solid light blue), and NADW (North Atlantic Deep Water, solid red). Exchange tracers are shown using hatched bars and are plotted adjacent to the ventilation tracer concentrations for each run. Exchange tracers are given by SW* (exchange Surface Water, purple with black hatches) and NADW* (exchange North Atlantic Deep Water, red with black hatches). Notice that NADW* includes NADW as well as the part of AABW that is sourced from former NADW* (and similarly for SW*).

where $b_{s_{min}}$ is the bottom of the surface layer defined as the minimum buoyancy in the top grid level at each latitude in the Southern Ocean (Figure 4).

The exchange tracer composition of the abyssal Indo-Pacific is broadly made up of similar parts SW* and NADW*, with weak spatial variations below the lower thermocline (~1000m) (Figure 4j-l). NADW* dominates the abyssal Indo-Pacific composition for the 0-2000m ridge cases (Figure 5). As ridge height increases past 2000m NADW* is gradually replaced by SW* in the abyssal Indo-Pacific until, by 3500m, NADW* makes up only about 25% of the abyssal Indo-Pacific tracer composition. The concentration of NADW* in the abyssal Indo-Pacific can be thought of as the sum of ventilation NADW that enters the abyssal Indo-Pacific directly at depth and the NADW*-derived AABW that is formed in the Southern Ocean. The proportion of AABW-derived NADW* in the abyssal Indo-Pacific (i.e. (NADW*-NADW)/NADW*) is high, ranging from approximately 91% for the 3000m ridge, low wind stress case to approximately 76% for the 0m ridge and 3500m ridge height cases under high wind stress, indicating that most NADW upwells in the Southern Ocean before making its way into the abyssal Indo-Pacific.

The decrease in abyssal Indo-Pacific NADW* concentrations with increasing ridge height is somewhat correlated with mid-depth cell strength, but the mid-depth cell strength does not capture the wind-stress-dependence of NADW* and the overall correlation is weaker than between venti-

Accepted for publication in *Journal of Physical Oceanography*. DOI 10.1175/JPO-D-23-0253.1.

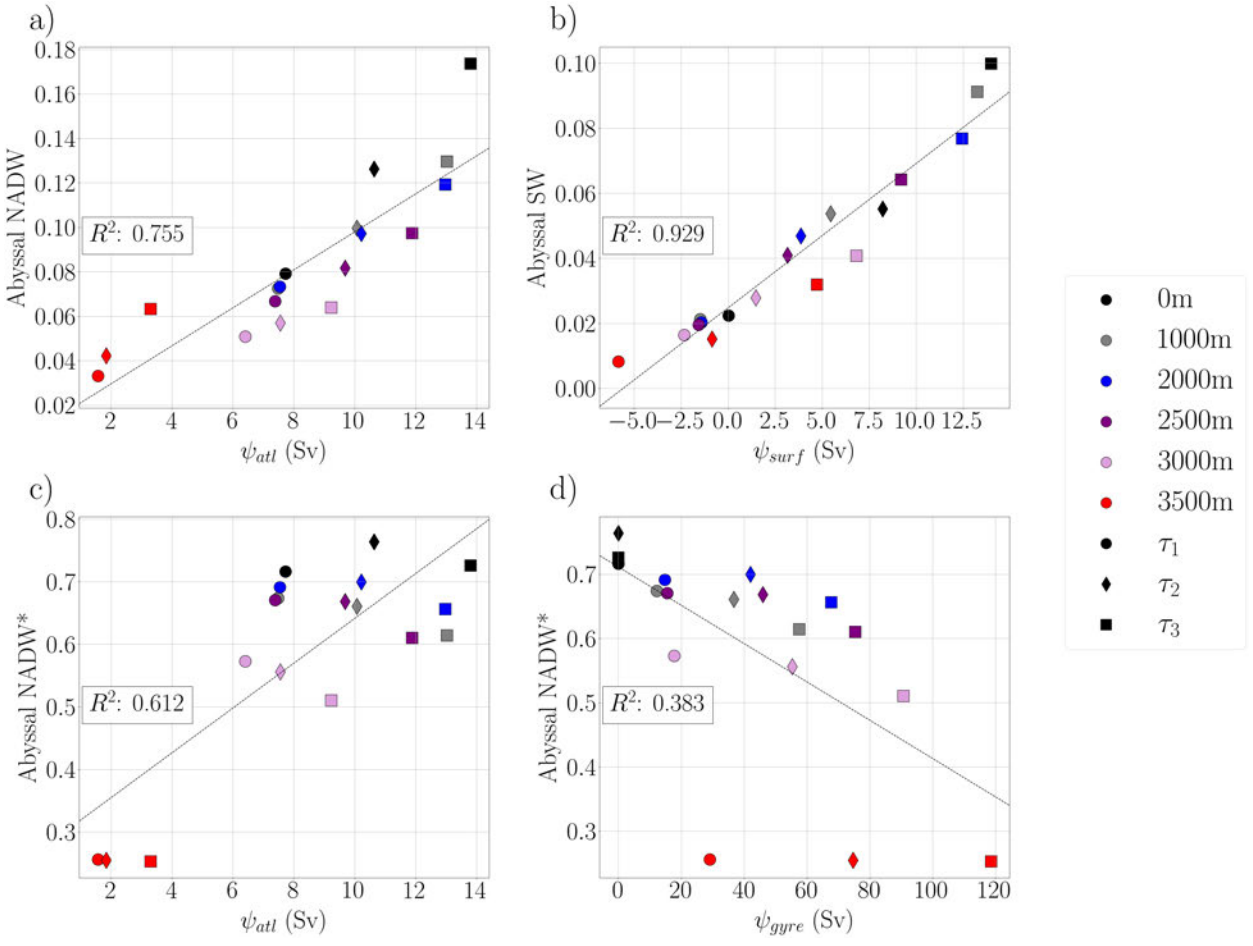

FIG. 6. a) Mean abyssal Indo-Pacific NADW concentrations vs mid-depth cell strength. b) Mean abyssal Indo-Pacific SW concentrations vs ψ_{surf}. c) Mean abyssal Indo-Pacific NADW* concentration vs mid-depth cell strength. d) Mean abyssal Indo-Pacific NADW* concentration vs gyre strength. The ridge height and wind stress used in each run is given by marker color and shape, respectively (see legend).

lation NADW and mid-depth cell strength (Figure 6c). In fact, much of the correlation between NADW* in the abyssal Indo-Pacific and ψ_{atl} can be explained by the strong concurrent fall off in both quantities in the 3500m ridge cases, suggesting that mid-depth cell strength alone is a poor predictor for exchange tracer concentration for low to intermediate ridge heights. Abyssal Indo-Pacific NADW* also exhibits a weak negative correlation with the strength of the Southern Ocean gyre (Figure 6d). As will be discussed in the following subsection, the variations in NADW* in the abyssal Indo-Pacific can be well described by the combined effect of the mid-depth cell and gyre strengths.

Accepted for publication in *Journal of Physical Oceanography*. DOI 10.1175/JPO-D-23-0253.1.

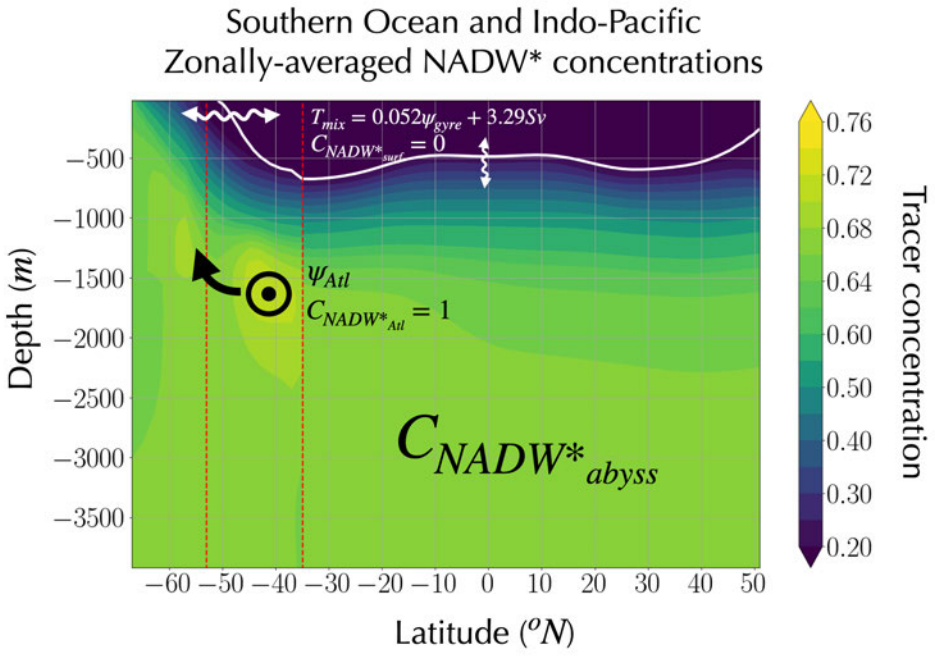

FIG. 7. Schematic illustrating our box model for the abyssal Indo-Pacific NADW* concentration, overlaid on the zonally-averaged C_{NADW^*} for the 2000m, $\tau_2 = 0.2N/m^2$ case. The white contour line in the upper ocean denotes the buoyancy level corresponding to the minimum buoyancy outcrop in the Southern Ocean, above which C_{NADW^*} is close to zero. White wavy arrows denote diapycnal exchange transport between the surface layer and the deep and abyssal ocean, and capture both vertical mixing in the ocean basin and horizontal mixing at the surface of the Southern Ocean. Net transport of NADW into the Southern Ocean and Indo-Pacific, ψ_{atl}, is shown by $\odot$ and corresponds to a maximum in zonally-averaged C_{NADW^*} in the Southern Ocean. Note that the C_{NADW^*} concentration in the abyssal ocean is fairly uniform throughout the deep and abyssal Southern Ocean and Indo-Pacific. Thin red dashed lines give the northern latitude of Drake Passage and the southern tip of Africa at 56^oS and 36^oS, respectively.

b. A simple model describing exchange tracer transport

The response of abyssal Indo-Pacific NADW* concentration to increasing ridge height and wind stress cannot be explained by any one transport process (Figure 6cd). With that in mind, we build a simple model based on conservation of tracer and mass that captures the variations in NADW* in the abyssal Indo-Pacific. The model considers a single volume comprised of the abyssal Indo-Pacific and Southern Ocean below the isopycnal $b_{SO_{min}}$ that outcrops at the northern end of the

Accepted for publication in *Journal of Physical Oceanography*. DOI 10.1175/JPO-D-23-0253.1.

Southern Ocean channel region (Figure 4), such that there is no surface restoring of NADW* (or SW*) within the volume. The concentration of abyssal Indo-Pacific NADW* (and thus SW*=1-NADW*) in this volume is thus governed by two processes: 1) mixing across the upper bounding isopycnal (both in the interior and at the surface of the Southern Ocean), which we characterize via an exchange transport T_{mix}, and 2) an advective source of NADW from the Atlantic with a rate ψ_{atl} (Figure 7). With T_{mix} and ψ_{atl} as the only two source terms that determine the ratio of NADW* and SW* in the abyssal ocean, we can construct a budget for the concentration of NADW* (c.f. Gebbie and Huybers 2010) in the abyssal Indo-Pacific ocean as:

$$C_{NADW^*_{abyss}} = \frac{\psi_{atl} C_{NADW^*_{atl}} + T_{mix} C_{NADW^*_{surf}}}{\psi_{atl} + T_{mix}}, \tag{8}$$

where ψ_{atl} is the strength of the mid-depth cell transport into the Southern Ocean as defined previously (Eq. 5), $C_{NADW^*_{atl}}$ and $C_{NADW^*_{surf}}$ are the time-mean concentrations of exchange NADW tracer in the incoming NADW and in the volume above $b_{SO_{min}}$, respectively, and $C_{NADW*_{abyss}}$ is the time-mean concentration of $NADW*$ in the abyssal Indo-Pacific (here taken below 2000m). Rearranging Eq. (8) and assuming the concentrations $C_{NADW^*_{surf}}$ and $C_{NADW^*_{atl}}$ are 0 and 1. respectively, we can derive a simple expression to infer the strength of T_{mix} from known quantities:

$$T_{mix} = \frac{\psi_{atl}(1 - C_{NADW^*_{abyss}})}{C_{NADW^*_{abyss}}}. \tag{9}$$

We find that T_{mix} is closely correlated with the strength of the Southern Ocean gyre (Figure 8a). As gyre strength increases the rate of the net diapycnal mixing transport increases as well, ranging from 3.1Sv in the 0m ridge cases where no gyre is present to 9.7Sv for the high wind stress, 3500m ridge case. A simple least-squares fit yields a linear scaling between T_{mix} and ψ_{gyre} of $T_{mix} = 0.052 \cdot \psi_{gyre} + 3.29Sv$, which matches the results with an R^2 value of 0.79. We note that T_{mix} necessarily includes contributions from both horizontal surface mixing across the ACC, which we expect to increase with the gyre strength, and interior diapycnal mixing, which is not expected to change much across our simulations and likely explains the constant offset in the least square fit. The relatively small interior diapycnal mixing-driven transport is consistent with our ventilation

Accepted for publication in *Journal of Physical Oceanography*. DOI 10.1175/JPO-D-23-0253.1.

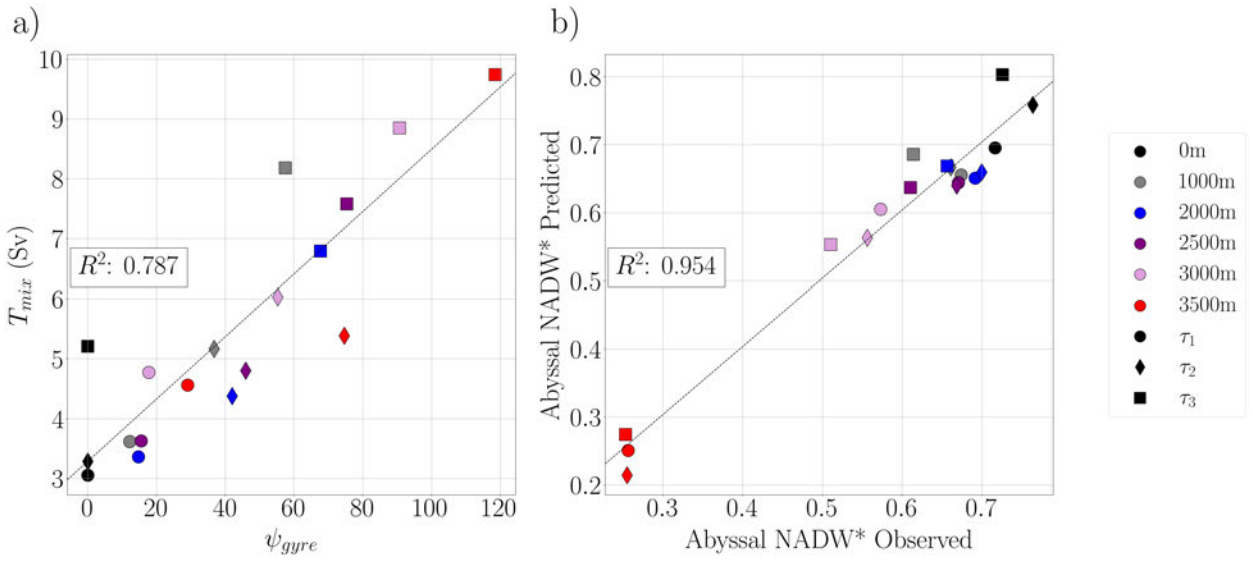

FIG. 8. a) T_{mix} estimated from Eq. Eq. (9) vs the strength of the Southern Ocean gyre. b) Predicted abyssal Indo-Pacific ocean NADW* concentrations derived from Eq. Eq. (10) vs the abyysal Indo-Pacific ocean NADW* concentrations simulated by our numerical models. As in Figure 6, the ridge height and wind stress used in each run is given by marker color and shape, respectively (see legend).

tracer results (Figure 4), which show very small SW ventilation tracer concentrations in the abyssal Pacific and with the majority of SW* consisting of former AABW.

Applying the scaling for T_{mix} with gyre strengths to Eq. (8) gives us a predictive model for the NADW* concentration in the abyssal Indo-Pacific ocean as a function of the mid-depth cell and gyre strength:

$$C_{NADW^*_{abyss}} = \frac{\psi_{atl}}{\psi_{atl} + 0.052 \cdot \psi_{gyre} + 3.29Sv}, \tag{10}$$

where the coefficients are determined from the linear scaling derived from Eq. (9). We find that Eq. (10) works well across all ridge cases and wind stress values, explaining about 95% of the variance in $C_{NADW*^*_{abyss}}$ (Figure 8b).

In summary, NADW* concentrations in the abyssal Indo-Pacific ocean decrease with a higher Drake Passage ridge and decreasing wind stress, a relationship that is primarily associated with the weakening mid-depth cell and the strengthening of the Southern Ocean gyre. The net transport of SW into the abyssal Indo-Pacific ocean that must balance NADW* injection by the mid-depth cell, T_{mix}, is highly correlated with the strength of the gyre south of the ACC. T_{mix}'s strong dependance

Accepted for publication in *Journal of Physical Oceanography*. DOI 10.1175/JPO-D-23-0253.1.

on the gyre circulation combined with the low concentration of ventilation SW in the abyssal ocean suggests that horizontal transport at the surface of the Southern Ocean plays a large role in setting the overall NADW* concentration, likely by exchanging NADW with surface waters north of the ACC.

5. Discussion

a. Limitations

The idealized configuration used in this study has allowed us to explore the mechanistic role of topographic barriers and wind stress in the Southern Ocean in affecting abyssal ocean water mass pathways. However, although this approach allows for relatively clean sensitivity experiments, care must be taken when interpreting our results in the context of the real ocean. In addition to the idealized topography, our model lacks salinity, which can modulate the circulation response via salt-advection feedbacks (e.g. Wolfe and Cessi 2014; Buckley and Marshall 2016; Ferreira et al. 2018), sea ice, which plays a key role in AABW formation (e.g. Ohshima et al. 2013; Jansen 2017), and coupled interactions with the atmosphere, which would further modulate the ocean boundary conditions. Our quantitative results are also specific to our model setup, as both basin width (Jones and Cessi 2017; Nadeau and Jansen 2020) and the configuration of the narrow ("Atlantic") basin (Ragen et al. 2022) can affect the rate of NADW and NADW* transport into the Southern Ocean via their influence on the strength and depth of the mid depth cell. The role of variations in the continental configuration, sea ice, and coupling to the atmosphere should be explored in future studies.

Our model's coarse resolution moreover requires mesoscale eddy effects to be parameterized, which is a major, but unfortunately unavoidable, limitation. Mesoscale eddies play an important role for the transport of tracers and buoyancy in the Southern Ocean (Sauermilch et al. 2021; Xing et al. 2023) and tend to be enhanced near topography (Abernathey and Cessi 2014; Patmore et al. 2019; Youngs et al. 2019; Wilson et al. 2022). Idealized studies of the Southern Ocean employing eddy-resolving models, such as Kong and Jansen (2021) and Xing et al. (2023), generally confirm that large standing meanders and gyres in the Southern Ocean play a dominant role in meridional heat transport, and also reduce the sensitivity of the "effective diffusivity" (i.e. the combined effect of standing and transient eddies) to the representation of mesoscale eddies, although some

Accepted for publication in *Journal of Physical Oceanography*. DOI 10.1175/JPO-D-23-0253.1.

sensitivity to eddy representation clearly remains (Kong and Jansen 2021). Resolved mesoscale eddies may also result in an enhancement of the Southern Ocean gyre strength (Sauermilch et al. 2021), an effect that could enhance the gyre-correlated mixing pathway we have identified in this study. Higher resolution may have additional influence in the presence of more advanced topography: Wilson et al. (2022), for example, found that a zonal ridge north of a subpolar gyre in the Southern Ocean (broadly representative of the Pacific-Antarctic Ridge in the real ocean) can reduce poleward heat transport by the gyre in an eddy-resolving simulation, although this effect is partially compensated by an increased southward transport by transient eddies across the zonal barrier.

In addition to our parameterization of mesoscale eddy effects, we use a constant vertical diffusivity which means that we are missing the potential effects of enhanced diapycnal mixing near topography (Mashayek et al. 2017). The effect of isopycnal and diapycnal mixing rates on abyssal watermass composition has previously been investigated by Jones and Abernathey (2019), who find that enhanced isopycnal mixing increases the AABW concentration relative to NADW in the abyssal ocean, while increased diapycnal mixing leads to gradual replacement of NADW and AABW by Indo-Pacific surface waters. We note that we generally find larger AABW concentrations and smaller NADW concentrations in the abyssal ocean than those found by Jones and Abernathey (2019) [3]. We attribute this distinction to different choices in model configuration between our two studies that influence the overall circulation – most notably, the setup employed by Jones and Abernathey (2019) generates a substantially deeper mid-depth cell, which likely explains the greater overall abundance of ventilation NADW in the abyssal ocean seen in their results.

Our limited resolution and simplified topographic setup also limits our ability to fully capture the complex circulation of the subpolar Southern Ocean gyres and other regional circulation features. Although the overall size of the gyre in our simulations (about $10-20^\circ$ in latitude and $20-50^\circ$ in longitude) is sufficiently large to be reasonably resolved in our model, the northward branch (which is effectively a western boundary current) is likely affected by the limited resolution and almost certainly affected by the details of the topography. The real Weddell Gyre, for example, is located in the lee of the outcropping Antarctic Peninsula and its northernmost zonal extant occurs farther to the east than in our simulations (Wunsch 2011). The real subpolar Southern Ocean moreover consists of an interconnected system of multiple gyres (Sonnewald et al. 2023), the cumulative

[3] Our "AABW" restoring domain is roughly equivalent to the combined "Channel" tracer restoring fields in Jones and Abernathey (2019)

Accepted for publication in *Journal of Physical Oceanography*. DOI 10.1175/JPO-D-23-0253.1.

effect of which is not explored here. Finally, the export of AABW and NADW* into the abyssal Indo-Pacific and thus their overall concentrations in the abyssal ocean may also be influenced by the specifics of Southern Ocean bottom topography (Solodoch et al. 2022). The empirical relationship between abyssal cell composition, ψ_{atl}, and ψ_{gyre} given by Eq. (10) is thus likely to look significantly different in the real ocean, and more work is needed to quantify the role of the gyre and other aspects of the subpolar Southern Ocean circulation under more realistic topography.

b. Implications

Our results highlight the role of Southern Ocean topography in affecting the pathways of abyssal water masses, an effect that is qualitatively consistent with previous studies. Specifically, the role of the gyre in modulating the prevalence of former NADW versus surface waters in the abyssal cell is broadly consistent with Talley (2013) and Reeve et al. (2019), who suggest that most of the upwelled NADW that enters the ACC is fed into bottom water formation regions near the Weddell and Ross Gyres along with entrained water masses that are able to cross the Subantarctic Front. The limited amount of direct NADW ventilation in the abyssal Indo-Pacific is consistent with the general picture of the modern day overturning circulation (i.e. Talley 2013; Lee et al. 2019), which suggests that most NADW entering the SO upwells before making its way into the Indo-Pacific as AABW. The strong relationship we observe between direct NADW ventilation in the abyssal Indo-Pacific and the strength of the mid-depth cell is expected, given the necessity of NADW to enter the Southern Ocean before it can make its way into the Indo-Pacific. The approximately linear relationship between ventilation NADW in the abyssal Indo-Pacific and mid-depth cell strength suggests that the proportion of NADW entering the Southern Ocean that makes it directly into the abyssal Indo-Pacific is relatively constant, although we note that this proportionality is likely to only hold for given rates of isopycnal and diapycnal mixing (c.f. Jones and Abernathey 2019). The relative concentration of NADW in the abyssal Indo-Pacific is also expected to be sensitive to the AABW formation rate (Li et al. 2023), which does not vary much across the simulations considered here.

The role of the Southern Ocean gyre in diluting upwelling NADW and shifting AABW composition may have implications for the climate during the Last Glacial Maximum (LGM). During the LGM the Southern Ocean is believed to have played a central role in reducing atmospheric

Accepted for publication in *Journal of Physical Oceanography*. DOI 10.1175/JPO-D-23-0253.1.

CO_2 (Broecker 1991; Sigman et al. 2010), with an expansion of permanent sea ice around Antarctica driving a shoaling of NADW, an isolation of the abyssal cell, and a subsequent reduction in atmospheric CO_2 as upwelling deep water remained insulated from the atmosphere and thus able to store carbon for a longer time (Stephens and Keeling 2000; Ferrari et al. 2014; Marzocchi and Jansen 2019; Nadeau et al. 2019). Our results suggest that a gyre-driven exchange between upwelling deep water and northern surface waters may alter the overall composition of the abyssal cell, a processes which could damp the effect of increased sea ice cover on abyssal carbon storage.

Our results may also shed light on the effects of the opening of Drake Passage on global ocean circulation and climate. Previous work has highlighted that the weakening of Southern Ocean Gyres with the widening of Drake Passage reduced poleward heat transport (Sauermilch et al. 2021). Potential further work could employ similar tracer experiments to investigate the role of the gyre in shaping interbasin exchange and the composition of AABW in past continental configurations.

It is important to note that the surface mixing accomplished here by the Southern Ocean gyre is not readily apparent in the zonally integrated MOC, which points to the limitations of relying on zonally-integrated theory or diagnostics to describe the structure of the ocean's large-scale circulation. This is particularly important when attempting to account for the net exchange of water masses between the mid-depth and abyssal cells. Previous work has suggested that the overlap between the mid-depth and abyssal cells in potential density space provides a key metric for the advective exchange between the mid-depth and abyssal cells (e.g. Ferrari et al. 2014; Nadeau et al. 2019; Baker et al. 2020; Nadeau and Jansen 2020). While our exchange tracer results do not directly measure the advective exchange between the mid-depth and abyssal cells, they suggest that the net transfer of tracers between NADW and the abyssal Indo-Pacific may be more affected by the overall strength of the mid-depth cell and the Southern Ocean gyres then by the overlap between the two overturning cells.

6. Summary and conclusions

In this work we have investigated the effect of topography and wind-forcing in the Southern Ocean on the composition of the abyssal ocean, using an idealized ocean GCM. As found in previous studies, the introduction of Southern Ocean topography results in changes to the large-

Accepted for publication in *Journal of Physical Oceanography*. DOI 10.1175/JPO-D-23-0253.1.

scale circulation, most notably a reduction in mid-depth cell strength and a gyre spin-up with increasing ridge height. We characterized the effect of these circulation changes on the abyssal ocean water mass composition in terms of 'ventilation' tracers that reflect the surface-origin of abyssal water masses and 'exchange' tracers that are allowed to circulate through the high-latitude Southern Ocean without being subject to surface restoring, thus allowing us to decompose AABW into former NADW versus water from lower latitude sources. Our main findings are summarized as follows:

- The mid depth cell is largely insensitive to Southern Ocean topography until the topographic height begins to intersect with the lower NADW isopycnals, after which mid depth cell strength drops substantially. The abyssal cell in the Indo-Pacific is largely insensitive to higher Drake Passage ridges until the very high (3500m) ridge case is reached.

- In our two-basin configuration the concentration of NADW tracer that directly enters the abyssal Indo-Pacific without contact with the surface is generally small (4-17%), indicating that relatively little NADW directly makes its way into the abyssal Indo-Pacific at depth.

- A large portion of the abyssal Indo-Pacific (26%-76%) is composed of "exchange" NADW (NADW*), indicating that a significant amount of NADW surfacing in the Southern Ocean enters the abyssal cell as AABW, although this fraction shows significant sensitivity to Southern Ocean topography and wind stress.

- Both the abyssal concentrations of NADW that reaches the abyssal Indo-Pacific directly and of NADW* decrease with increasing ridge height and decreasing Southern Ocean wind stress.

- The changing abyssal concentrations of NADW and NADW* in the Indo-Pacific can be explained primarily by the weakening of the mid-depth cell in the South Atlantic, whereby less NADW makes it out of the Atlantic, and secondarily by the strengthening of the Southern Ocean gyre,whereby upwelling NADW* is exchanged with thermocline and intermediate waters from the northern basins.

Our results highlight the combined role of the mid-depth cell and the Southern Ocean gyre circulation in controlling the transport of tracers into the abyssal Indo-Pacific, a finding that has implications for both our conceptual picture of the current overturning circulation and for abyssal

Accepted for publication in *Journal of Physical Oceanography*. DOI 10.1175/JPO-D-23-0253.1.

ocean tracers and carbon storage in past and future climates. However, more work is needed to quantify the role of these mechanisms in more realistic model configurations and in the real ocean.

Acknowledgments. Computational resources for this project were generously provided by the University of Chicago Research Computing Center. We acknowledge support from the National Science Foundation (NSF) through Award OCE-1846821.

Data availability statement. The MITgcm configuration used for this paper, model output, and example analysis scripts are available on Zenodo (10.5281/zenodo.10393455).

Accepted for publication in *Journal of Physical Oceanography*. DOI 10.1175/JPO-D-23-0253.1.

References

Abernathey, R., and P. Cessi, 2014: Topographic enhancement of eddy efficiency in baroclinic equilibration. *Journal of Physical Oceanography*, **44 (8)**, 2107 – 2126, https://doi.org/10.1175/JPO-D-14-0014.1.

Abernathey, R., J. Marshall, and D. Ferreira, 2011: The dependence of southern ocean meridional overturning on wind stress. *Journal of Physical Oceanography*, **41 (12)**, 2261 – 2278, https://doi.org/10.1175/JPO-D-11-023.1.

Anagnostou, E., and Coauthors, 2016: Changing atmospheric co2 concentration was the primary driver of early cenozoic climate. *Nature*, **533 (7603)**, 380–384, https://doi.org/10.1038/nature17423.

Anderson, R., A. S, L. Bradtmiller, S. Nielsen, M. Fleisher, B. Anderson, and L. Burckle, 2009: Wind-driven upwelling in the Southern Ocean and the deglacial rise in atmospheric CO2. *Science*, **323 (5920)**, 1443–1448, https://doi.org/10.1126/science.1167441.

Baker, J. A., A. J. Watson, and G. K. Vallis, 2020: Meridional overturning circulation in a multibasin model. Part I: Dependence on Southern Ocean buoyancy forcing. *Journal of Physical Oceanography*, **50 (5)**, 1159 – 1178, https://doi.org/10.1175/JPO-D-19-0135.1.

Bishop, S. P., P. R. Gent, F. O. Bryan, A. F. Thompson, M. C. Long, and R. Abernathey, 2016: Southern Ocean overturning compensation in an eddy-resolving climate simulation. *Journal of Physical Oceanography*, **46 (5)**, 1575 – 1592, https://doi.org/10.1175/JPO-D-15-0177.1.

Broecker, W. S., 1991: The great ocean conveyor. *Oceanography*, **4 (2)**, 79–89, https://doi.org/10.5670/oceanog.1991.07.

Bryan, F., 1986: High-latitude salinity effects and interhemispheric thermohaline circulations. *Nature*, **323 (6086)**, 301–304, https://doi.org/10.1038/323301a0.

Buckley, M. W., and J. Marshall, 2016: Observations, inferences, and mechanisms of the atlantic meridional overturning circulation: A review. *Reviews of Geophysics*, **54 (1)**, 5–63, https://doi.org/https://doi.org/10.1002/2015RG000493.

Accepted for publication in *Journal of Physical Oceanography*. DOI 10.1175/JPO-D-23-0253.1.

Cessi, P., 2019: The global overturning circulation. *Annual Review of Marine Science*, **11 (1)**, 249–270, https://doi.org/10.1146/annurev-marine-010318-095241.

Chang, C.-Y., and M. F. Jansen, 2021: Distinct controls on the strength of the abyssal overturning circulation: Channel versus basin dynamics. *Journal of Physical Oceanography*, **51 (7)**, 2073 – 2086, https://doi.org/10.1175/JPO-D-20-0316.1.

de Boer, A. M., D. K. Hutchinson, F. Roquet, L. C. Sime, N. J. Burls, and C. Heuzé, 2022: The impact of southern ocean topographic barriers on the ocean circulation and the overlying atmosphere. *Journal of Climate*, **35 (18)**, 5805–5821, https://doi.org/https://doi.org/10.1175/JCLI-D-21-0896.1.

Dotto, T. S., and Coauthors, 2018: Variability of the ross gyre, southern ocean: Drivers and responses revealed by satellite altimetry. *Geophysical Research Letters*, **45 (12)**, 6195–6204, https://doi.org/https://doi.org/10.1029/2018GL078607.

Ferrari, R., and D. Ferreira, 2011: What processes drive the ocean heat transport? *Ocean Modelling*, **38 (3-4)**, 171–186, https://doi.org/10.1016/j.ocemod.2011.02.013.

Ferrari, R., M. Jansen, J. Adkins, A. Burke, A. Stewart, and A. Thompson, 2014: Antarctic sea ice control on ocean circulation in present and glacial climates. *Proceedings of the National Academy of Sciences*, **111 (24)**, 8753–8758, https://doi.org/10.1073/pnas.1323922111.

Ferrari, R., L. Nadeau, D. P. Marshall, L. C. Allison, and H. L. Johnson, 2017: A model of the ccean circulation with two closed basins and a reentrant channel. *Journal of Physical Oceanography*, **47 (12)**, 2887–2906, https://doi.org/10.1175/JPO-D-16-0223.1.

Ferreira, D., and Coauthors, 2018: Atlantic-pacific asymmetry in deep water formation. *Annual Review of Earth and Planetary Sciences*, **46 (Volume 46, 2018)**, 327–352, https://doi.org/https://doi.org/10.1146/annurev-earth-082517-010045.

Gebbie, G., and P. Huybers, 2010: Total matrix intercomparison: A method for determining the geometry of water-mass pathways. *Journal of Physical Oceanography*, **40 (8)**, 1710 – 1728, https://doi.org/10.1175/2010JPO4272.1.

Accepted for publication in *Journal of Physical Oceanography*. DOI 10.1175/JPO-D-23-0253.1.

Gent, P. R., and J. C. Mcwilliams, 1990: Isopycnal mixing in ocean circulation models. *Journal of Physical Oceanography*, **20**, 150–155, https://doi.org/10.1175/1520-0485(1990)020⟨0150:IMIOCM⟩2.0.CO;2.

Gnanadesikan, A., 1999: A simple predictive model for the structure of the oceanic pycnocline. *Science*, **283 (5410)**, 2077–2079, https://doi.org/10.1126/science.283.5410.2077.

Goldner, A., N. Herold, and M. Huber, 2014: Antarctic glaciation caused ocean circulation changes at the eocene–oligocene transition. *Nature*, **511 (7511)**, 574–577, https://doi.org/10.1038/nature13597.

Haine, T. W. N., and T. M. Hall, 2002: A generalized transport theory: water-mass composition and age. *Journal of Physical Oceanography*, **32 (6)**, 1932 – 1946, https://doi.org/10.1175/1520-0485(2002)032⟨1932:AGTTWM⟩2.0.CO;2.

Ito, T., M. Woloszyn, and M. Mazloff, 2010: Anthropogenic carbon dioxide transport in the southern ocean driven by ekman flow. *Nature*, **463 (7277)**, 80–83, https://doi.org/10.1038/nature08687.

Jansen, M. F., 2017: Glacial ocean circulation and stratification explained by reduced atmospheric temperature. *Proceedings of the National Academy of Sciences*, **114 (1)**, 45–50, https://doi.org/10.1073/pnas.1610438113.

Jones, C. S., and R. Abernathey, 2019: Isopycnal mixing controls deep ocean ventilation. *Geophysical Research Letters*, **46 (22)**, 13 144–13 151, https://doi.org/10.1029/2019GL085208.

Jones, C. S., and P. Cessi, 2016: Interbasin transport of the meridional overturning circulation. *Journal of Physical Oceanography*, 1157–1169, https://doi.org/10.1175/JPO-D-15-0197.1.

Jones, C. S., and P. Cessi, 2017: Size matters: Another reason why the atlantic is saltier than the pacific. *Journal of Physical Oceanography*, **47 (11)**, 2843–2859, https://doi.org/https://doi.org/10.1175/JPO-D-17-0075.1.

Kennedy, A. T., A. Farnsworth, D. J. Lunt, C. H. Lear, and P. J. Markwick, 2015: Atmospheric and oceanic impacts of antarctic glaciation across the eocene–oligocene transition. *Philosophical Transactions of the Royal Society A: Mathematical, Physical and Engineering Sciences*, **373 (2054)**, 20140 419, https://doi.org/10.1098/rsta.2014.0419.

Accepted for publication in *Journal of Physical Oceanography*. DOI 10.1175/JPO-D-23-0253.1.

Kennett, J. P., 1977: Cenozoic evolution of antarctic glaciation, the circum-antarctic ocean, and their impact on global paleoceanography. *Journal of Geophysical Research (1896-1977)*, **82 (27)**, 3843–3860, https://doi.org/https://doi.org/10.1029/JC082i027p03843.

Kong, H., and M. F. Jansen, 2021: The impact of topography and eddy parameterization on the simulated Southern Ocean circulation response to changes in surface wind stress. *Journal of Physical Oceanography*, **51 (3)**, 825 – 843, https://doi.org/10.1175/JPO-D-20-0142.1.

Lee, S.-K., R. Lumpkin, M. O. Baringer, C. S. Meinen, M. Goes, S. Dong, H. Lopez, and S. G. Yeager, 2019: Global meridional overturning circulation inferred from a data-constrained ocean & sea-ice model. *Geophysical Research Letters*, **46 (3)**, 1521–1530, https://doi.org/10.1029/2018GL080940.

Li, L., Z. Liu, J. Du, L. Wan, and J. Lu, 2023: Mechanisms of global ocean ventilation age change during the last deglaciation. *EGUsphere*, **2023**, 1–25, https://doi.org/10.5194/egusphere-2023-2256.

Lumpkin, and Speer, 2007: Global ocean meridional overturning. *Journal of Physical Oceanography*, **37 (10)**, 2550–2562, https://doi.org/10.1175/JPO3130.1.

Mak, J., J. R. Maddison, D. P. Marshall, and D. R. Munday, 2018: Implementation of a geometrically informed and energetically constrained mesoscale eddy parameterization in an ocean circulation model. *Journal of Physical Oceanography*, **48 (10)**, 2363–2382, https://doi.org/https://doi.org/10.1175/JPO-D-18-0017.1.

Marshall, J., A. J. Adcroft, C. Hill, L. T. Perelman, and C. W. Heisey, 1997: A finite-volume, incompressible navier stokes model for studies of the ocean on parallel computers. *Journal of Geophysical Research*, **102**, 5753–5766, https://doi.org/10.1029/96JC02775.

Marshall, J., and T. Radko, 2003: Residual-mean solutions for the Antarctic circumpolar current and its associated overturning circulation. *Journal of Physical Oceanography*, **33 (11)**, 2341 – 2354, https://doi.org/10.1175/1520-0485(2003)033⟨2341:RSFTAC⟩2.0.CO;2.

Marshall, J., and K. Speer, 2012: Closure of the meridional overturning circulation through Southern Ocean upwelling. *Nature Geoscience*, **5 (3)**, 171–181, https://doi.org/10.1038/ngeo1391.

Accepted for publication in *Journal of Physical Oceanography*. DOI 10.1175/JPO-D-23-0253.1.

Marzocchi, A., and M. F. Jansen, 2019: Global cooling linked to increased glacial carbon storage via changes in Antarctic sea ice. *Nature Geoscience*, **12 (12)**, 1001–1005, https://doi.org/10.1038/s41561-019-0466-8.

Mashayek, A., R. Ferrari, S. Merrifield, J. R. Ledwell, L. St Laurent, and A. N. Garabato, 2017: Topographic enhancement of vertical turbulent mixing in the southern ocean. *Nature Communications*, **8 (1)**, 14 197, https://doi.org/10.1038/ncomms14197.

Mazloff, M. R., P. Heimbach, and C. Wunsch, 2010: An eddy-permitting southern ocean state estimate. *Journal of Physical Oceanography*, **40 (5)**, 880–899, https://doi.org/https://doi.org/10.1175/2009JPO4236.1.

Munk, W. H., and E. Palmén, 1951: Note on the dynamics of the antarctic circumpolar current1. *Tellus*, **3 (1)**, 53–55, https://doi.org/https://doi.org/10.1111/j.2153-3490.1951.tb00776.x.

Nadeau, L., R. Ferrari, and M. F. Jansen, 2019: Antarctic sea ice control on the depth of North Atlantic deep water. *Journal of Climate*, **32 (9)**, 2537–2551, https://doi.org/10.1175/JCLI-D-18-0519.1.

Nadeau, L., and M. F. Jansen, 2020: Overturning circulation pathways in a two-basin ocean model. *American Meteorlogical Society*, **50**, 2105–2122, https://doi.org/10.1175/JPO-D-20-0034.s1.

Nadeau, L.-P., and R. Ferrari, 2015: The role of closed gyres in setting the zonal transport of the antarctic circumpolar current. *Journal of Physical Oceanography*, **45 (6)**, 1491 – 1509, https://doi.org/10.1175/JPO-D-14-0173.1.

Nikurashin, M., and G. Vallis, 2012: A theory of the interhemispheric meridional overturning circulation and associated stratification. *Journal of Physical Oceanography*, **42 (10)**, 1652 – 1667, https://doi.org/10.1175/JPO-D-11-0189.1.

Nurser, A. J. G., and M.-M. Lee, 2004: Isopycnal averaging at constant height. Part II: Relating to the residual streamfunction in eulerian space. *Journal of Physical Oceanography*, **34 (12)**, 2740 – 2755, https://doi.org/10.1175/JPO2650.1.

Ohshima, K. I., and Coauthors, 2013: Antarctic bottom water production by intense sea-ice formation in the cape darnley polynya. *Nature Geoscience*, **6 (3)**, 235–240, https://doi.org/10.1038/ngeo1738.

Accepted for publication in *Journal of Physical Oceanography*. DOI 10.1175/JPO-D-23-0253.1.

Olbers, D., 1998: Comments on "on the obscurantist physics of 'form drag'in theorizing about the circumpolar current. *Journal of Physical Oceanography*, **28 (8)**, 1647–1654, https://doi.org/ https://doi.org/10.1175/1520-0485(1998)028⟨1647:COOTOP⟩2.0.CO;2.

Patmore, R. D., P. R. Holland, D. R. Munday, A. C. N. Garabato, D. P. Stevens, and M. P. Meredith, 2019: Topographic control of Southern Ocean gyres and the Antarctic circumpolar current: A barotropic perspective. *Journal of Physical Oceanography*, **49 (12)**, 3221 – 3244, https://doi.org/10.1175/JPO-D-19-0083.1.

Prather, M. J., 1986: Numerical advection by conservation of second-order moments. *Journal of Geophysical Research: Atmospheres*, **91 (D6)**, 6671–6681, https://doi.org/10.1029/ JD091iD06p06671.

Primeau, F., 2005: Characterizing transport between the surface mixed layer and the ocean interior with a forward and adjoint global ocean transport model. *Journal of Physical Oceanography*, **35 (4)**, 545 – 564, https://doi.org/10.1175/JPO2699.1.

Ragen, S., K. C. Armour, L. Thompson, A. Shao, and D. Darr, 2022: The role of atlantic basin geometry in meridional overturning circulation. *Journal of Physical Oceanography*, **52 (3)**, 475–492, https://doi.org/https://doi.org/10.1175/JPO-D-21-0036.1.

Redi, M. H., 1982: Oceanic isopycnal mixing by coordinate rotation. *Journal of Physical Oceanography*, **12**, 1154–1158, https://doi.org/10.1175/1520-0485(1982)012⟨1154:OIMBCR⟩2.0.CO;2.

Reeve, K. A., O. Boebel, V. Strass, T. Kanzow, and R. Gerdes, 2019: Horizontal circulation and volume transports in the Weddell Gyre derived from Argo float data. *Progress in Oceanography*, **175**, 263–283, https://doi.org/10.1016/j.pocean.2019.04.006.

Ridgway, K. R., and J. R. Dunn, 2007: Observational evidence for a southern hemisphere oceanic supergyre. *Geophysical Research Letters*, **34 (13)**, https://doi.org/https://doi.org/10. 1029/2007GL030392.

Sauermilch, I., J. M. Whittaker, A. Klocker, D. R. Munday, K. Hochmuth, P. K. Bijl, and J. H. LaCasce, 2021: Gateway-driven weakening of ocean gyres leads to southern ocean cooling. *Nature Communications*, **12 (1)**, 6465, https://doi.org/10.1038/s41467-021-26658-1.

Accepted for publication in *Journal of Physical Oceanography*. DOI 10.1175/JPO-D-23-0253.1.

Schmidgall, C. R., Y. Si, A. L. Stewart, A. F. Thompson, and A. M. Hogg, 2023: Dynamical controls on bottom water transport and transformation across the antarctic circumpolar current. *Journal of Physical Oceanography*, **53 (8)**, 1917–1940, https://doi.org/https://doi.org/10.1175/JPO-D-22-0113.1.

Schröder, M., and E. Fahrbach, 1999: On the structure and the transport of the eastern Weddell Gyre. *Deep Sea Research Part II: Topical Studies in Oceanography*, **46 (1)**, 501–527, https://doi.org/10.1016/S0967-0645(98)00112-X.

Shakespeare, C. J., and A. M. Hogg, 2012: An analytical model of the response of the meridional overturning circulation to changes in wind and buoyancy forcing. *Journal of Physical Oceanography*, **42 (8)**, 1270 – 1287, https://doi.org/10.1175/JPO-D-11-0198.1.

Sigman, D. M., M. P. Hain, and G. H. Haug, 2010: The polar ocean and glacial cycles in atmospheric CO2 concentration. *Nature*, **466 (7302)**, 47–55, https://doi.org/10.1038/nature09149.

Sijp, W. P., and M. H. England, 2004: Effect of the drake passage throughflow on global climate. *Journal of Physical Oceanography*, **34 (5)**, 1254–1266, https://doi.org/https://doi.org/10.1175/1520-0485(2004)034⟨1254:EOTDPT⟩2.0.CO;2.

Solodoch, A., A. L. Stewart, A. M. Hogg, A. K. Morrison, A. E. Kiss, A. F. Thompson, S. G. Purkey, and L. Cimoli, 2022: How does antarctic bottom water cross the southern ocean? *Geophysical Research Letters*, **49 (7)**, e2021GL097 211, https://doi.org/https://doi.org/10.1029/2021GL097211.

Sonnewald, M., K. A. Reeve, and R. Lguensat, 2023: A southern ocean supergyre as a unifying dynamical framework identified by physics-informed machine learning. *Communications Earth & Environment*, **4 (1)**, 153, https://doi.org/10.1038/s43247-023-00793-7.

Speich, S., B. Blanke, and W. Cai, 2007: Atlantic meridional overturning circulation and the southern hemisphere supergyre. *Geophysical Research Letters*, **34 (23)**, https://doi.org/https://doi.org/10.1029/2007GL031583.

Srokosz, M., M. Baringer, H. Bryden, S. Cunningham, T. Delworth, S. Lozier, J. Marotzke, and R. Sutton, 2012: Past, present, and future changes in the Atlantic meridional overturning circu-

Accepted for publication in *Journal of Physical Oceanography*. DOI 10.1175/JPO-D-23-0253.1.

lation. *Bulletin of the American Meteorological Society*, **93 (11)**, 1663 – 1676, https://doi.org/10.1175/BAMS-D-11-00151.1.

Stephens, B. B., and R. F. Keeling, 2000: The influence of Antarctic sea ice on glacial–interglacial CO2 variations. *Nature*, **404 (6774)**, 171–174, https://doi.org/10.1038/35004556.

Stewart, A. L., and A. M. Hogg, 2017: Reshaping the Antarctic circumpolar current via Antarctic bottom water export. *Journal of Physical Oceanography*, **47 (10)**, 2577 – 2601, https://doi.org/10.1175/JPO-D-17-0007.1.

Stewart, A. L., N. K. Neumann, and A. Solodoch, 2023: "eddy"saturation of the antarctic circumpolar current by standing waves. *Journal of Physical Oceanography*, **53 (4)**, 1161–1181, https://doi.org/https://doi.org/10.1175/JPO-D-22-0154.1.

Talley, L., 2013: Closure of the global overturning circulation through the Indian, Pacific, and Southern oceans: Schematics and transports. *Oceanography*, **26 (1)**, 80–97, https://doi.org/10.5670/oceanog.2013.07.

Tamsitt, V., and Coauthors, 2017: Spiraling pathways of global deep waters to the surface of the Southern Ocean. *Nature Communications*, **8 (1)**, 172, https://doi.org/10.1038/s41467-017-00197-0.

Thompson, A., A. Stewart, and T. Bischoff, 2016: A multibasin residual-mean model for the global overturning circulation. *Journal of Physical Oceanography*, **46 (9)**, 2583–2604, https://doi.org/10.1175/JPO-D-15-0204.1.

Thompson, A. F., and A. C. N. Garabato, 2014: Equilibration of the Antarctic circumpolar current by standing meanders. *Journal of Physical Oceanography*, **44 (7)**, 1811 – 1828, https://doi.org/10.1175/JPO-D-13-0163.1.

Toggweiler, J., J. L. Russell, and S. R. Carson, 2006: Midlatitude westerlies, atmospheric CO2, and climate change during the ice ages. *Paleooceanography*, **21 (PA2005)**, https://doi.org/10.1029/2005PA001154.

Toggweiler, J., and B. Samuels, 1995a: Effect of Drake Passage on the global thermohaline circulation. *Deep Sea Research Part I: Oceanographic Research Papers*, **42 (4)**, 477–500, https://doi.org/10.1016/0967-0637(95)00012-U.

Accepted for publication in *Journal of Physical Oceanography*. DOI 10.1175/JPO-D-23-0253.1.

Toggweiler, J. R., and H. Bjornsson, 2000: Drake passage and palaeoclimate. *Journal of Quaternary Science*, **15 (4)**, 319–328, https://doi.org/https://doi.org/10.1002/1099-1417(200005)15:4⟨319::AID-JQS545⟩3.0.CO;2-C.

Toggweiler, J. R., and B. Samuels, 1995b: Effect of drake passage on the global thermohaline circulation. *Deep Sea Research Part I: Oceanographic Research Papers*, **42 (4)**, 477–500, https://doi.org/https://doi.org/10.1016/0967-0637(95)00012-U.

Toumoulin, A., Y. Donnadieu, J. B. Ladant, S. J. Batenburg, F. Poblete, and G. Dupont-Nivet, 2020: Quantifying the effect of the drake passage opening on the eocene ocean. *Paleoceanography and Paleoclimatology*, **35 (8)**, e2020PA003 889, https://doi.org/https://doi.org/10.1029/2020PA003889.

Vallis, G. K., 2000: Large-scale circulation and production of stratification: Effects of wind, geometry, and diffusion. *Journal of Physical Oceanography*, **30 (5)**, 933 – 954, https://doi.org/10.1175/1520-0485(2000)030⟨0933:LSCAPO⟩2.0.CO;2.

Walin, G., 1982: On the relation between sea-surface heat flow and thermal circulation in the ocean. *Tellus*, **34 (2)**, 187–195, https://doi.org/10.1111/j.2153-3490.1982.tb01806.x.

Wang, Z., 2013: On the response of southern hemisphere subpolar gyres to climate change in coupled climate models. *Journal of Geophysical Research: Oceans*, **118 (3)**, 1070–1086, https://doi.org/10.1002/jgrc.20111.

Wilson, E. A., A. F. Thompson, A. L. Stewart, and S. Sun, 2022: Bathymetric control of subpolar gyres and the overturning circulation in the Southern Ocean. *Journal of Physical Oceanography*, **52 (2)**, 205 – 223, https://doi.org/10.1175/JPO-D-21-0136.1.

Wolfe, and Cessi, 2011: The adiabatic pole-to-pole overturning circulation. *Journal of Physical Oceanography*, **41 (9)**, 1795–1810, https://doi.org/10.1175/2011JPO4570.1.

Wolfe, C. L., and P. Cessi, 2014: Salt feedback in the adiabatic overturning circulation. *Journal of Physical Oceanography*, **44 (4)**, 1175–1194, https://doi.org/https://doi.org/10.1175/JPO-D-13-0154.1.

Wunsch, C., 2011: The decadal mean ocean circulation and sverdrup balance. *Journal of Marine Research*, **69**, 417–434.

Accepted for publication in *Journal of Physical Oceanography*. DOI 10.1175/JPO-D-23-0253.1.

Xing, Q., A. Klocker, D. Munday, and J. Whittaker, 2023: Deepening of Southern Ocean gateway leads to abrupt onset of a deep-reaching meridional overturning circulation. *Geophysical Research Letters*, **50 (19)**, e2023GL104 382, https://doi.org/10.1029/2023GL104382.

Youngs, M. K., and G. R. Flierl, 2023: Extending residual-mean overturning theory to the topographically localized transport in the Southern Ocean. *Journal of Physical Oceanography*, **53 (8)**, 1901 – 1915, https://doi.org/10.1175/JPO-D-22-0217.1.

Youngs, M. K., G. R. Flierl, and R. Ferrari, 2019: Role of residual overturning for the sensitivity of southern ocean isopycnal slopes to changes in wind forcing. *Journal of Physical Oceanography*, **49 (11)**, 2867–2881, https://doi.org/https://doi.org/10.1175/JPO-D-19-0072.1.

Zachos, J., M. Pagani, L. Sloan, E. Thomas, and K. Billups, 2001: Trends, rhythms, and aberrations in global climate 65 ma to present. *Science*, **292 (5517)**, 686–693, https://doi.org/10.1126/science.1059412.

Accepted for publication in *Journal of Physical Oceanography*. DOI 10.1175/JPO-D-23-0253.1.